Journal of Food Engineering xxx (2017) 1–8

Contents lists available at ScienceDirect

Journal of Food Engineering

journal homepage: www.elsevier.com/locate/jfoodeng

Design and characterisation of food grade powders and inks for microstructure control using 3D printing☆

Sonia Holland [a, b, *], Tim Foster [a], William MacNaughtan [a], Chris Tuck [b]

[a] Division of Food Science, Sutton Bonington Campus, University of Nottingham, Loughborough LE12 5RD, United Kingdom
[b] 3D Printing and Additive Manufacturing Research Group, University Park, University of Nottingham, Nottingham NG7 2RD, United Kingdom

ARTICLE INFO

Article history:
Received 16 September 2016
Received in revised form
5 June 2017
Accepted 7 June 2017
Available online xxx

Keywords:
Binder jetting
Amorphous cellulose
Polysaccharides

ABSTRACT

Additive Manufacturing techniques have been previously applied to food materials with direct consumption in mind, as opposed to creating structural ingredients as shown in this study. First, semi-crystalline cellulose was mechanically treated by ball milling to render an amorphous powder, which has been characterised. Requirements for the subsequent recrystallization of this powder with a view to structuring have been determined through the control of moisture and thermal energy. Food inks based on xanthan gum have been formulated to enable successful jetting with a FujiFilm Dimatix ink jet printer. The polymer inks were subsequently jetted onto the amorphous cellulose powder to observe powder-binder interactions. Material combinations and parameters were optimised to produce cohesive geometric structures. The results of this study are promising when looking towards using these materials in a binder jetting additive manufacturing technique using designer particles and inks to create structures for use in food products.

© 2017 The Authors. Published by Elsevier Ltd. This is an open access article under the CC BY license (http://creativecommons.org/licenses/by/4.0/).

1. Introduction

Mass customisation, geometric design freedom, low volume economy and less processing waste are key benefits that Additive Manufacturing (AM, often referred to as 3D printing) technology provides to other platforms which could be advantageous in the food industry. The application of AM to food materials is unusual due to the open source nature and hobbyist culture stemming from a relative ease to source hardware, as well as experimental interest from academic institutions, large companies, small start-ups and laymen – thus many developments are not formally documented. Key reviews by Godoi et al. (2016), Lipton et al. (2015), Sun et al. (2015) and Wegrzyn et al. (2012) provide insight into current developments by a number of parties into AM of food materials. Though material feedstocks and processes differ among the various applications they have a common thread; all end use products are designed on the macro scale for direct consumption or post process cooking by the consumer. In these instances the freedom of design complexity is being utilised but with end consumer wants in mind. More recent publications are indicative of the many facets of food printing that are beginning to emerge such as its use as an educational tool (Hamilton et al., 2017), to enable molecular gastronomic creations (D'Angelo et al., 2016), to influence food textural properties (Le Tohic et al., 2017) and even provide a cheap, sacrificial material feedstock for 'lab-on-a-chip' capabilities when combined with PDMS (He et al., 2015). Similarly, 3D Printing technology options for food materials are beginning to be discussed to suit specific processing needs (Sun et al., 2017). Food systems are complex; microstructures determining textural attributes, stability and flavour release typically arise through interaction and self-assembly of components during processing. If AM technology were to be truly exploited by the food industry it would be advantageous to achieve this intricacy on more relevant, smaller length scales within food products.

There are seven categories of AM recognised as per the ASTM standard terminology for Additive Manufacturing Technologies (ASTM International, 2015). The AM technology commonly used for food products involves material extrusion from a nozzle, therefore a limiting factor for feature size is the nozzle diameter used. Taking into account the multi-component nature of the ingredient feedstock as a potential for blockages and probable negative effects caused by pressure and shear on extrusion of the material, nozzle

☆ This work was supported by the Engineering and Physical Sciences Research Council [grant numbers EP/I033335/2, EP/K030957/1]; and a gift by the University of Nottingham.

* Corresponding author.
E-mail address: Sonia.Holland@nottingham.ac.uk (S. Holland).

http://dx.doi.org/10.1016/j.jfoodeng.2017.06.008
0260-8774/© 2017 The Authors. Published by Elsevier Ltd. This is an open access article under the CC BY license (http://creativecommons.org/licenses/by/4.0/).

Please cite this article in press as: Holland, S., et al., Design and characterisation of food grade powders and inks for microstructure control using 3D printing, Journal of Food Engineering (2017), http://dx.doi.org/10.1016/j.jfoodeng.2017.06.008

diameters are typically greater than 1 mm and rarely below 0.5 mm, unless feedstock homogeneity and print viscosity can be assured. Thus this is the minimum feature size for products produced; often layering adhesion sites are visible to the naked eye in the z direction.

Binder jetting is a category of AM in which a liquid binder is ink-jetted onto a powder base in cross sectional layers based on the digital design file. Once one layer is printed, a roller or blade deposits a fresh layer of powder for the next cross sectional design to be jetted on to, as depicted in Fig. 1. This sequential layering and jetting process is continued until, encased in surrounding unbound powder, the adhered structure, which is handleable, may be removed from the powder bed. Ink jet nozzles can deposit as little as 1 pL of ink per droplet, but are typically 10 pL when a 21 μm diameter nozzle is used.

The powder component is ideally bimodal or multimodal to allow for ease of spreading as well as to enhance adhesion. Smaller particles will fill the gaps created between larger particles creating more potential junction zones, ultimately reducing unwanted porosity in the finished product. Depending on the application or desired minimum feature size the d_{50} (particle diameter at 50% in the cumulative distribution) of the powder can range from 100 μm to below 20 μm. It has been suggested that use of particle blends with d_{50} between 30 and 100 μm gives higher mechanical strength than finer particles (Shirazi et al., 2015). In addition, using particles with a size range 80–150 μm, which is close to the intended layer thickness, or those below 5 μm, inducing Van der Waals mediated agglomeration, is also likely to have detrimental effects on print quality (Vorndran et al., 2015).

Binding materials must be designed in such a way that droplets ejected achieve the correct form (spherical, without a trailing ligament or non-merging satellite droplets) and at sufficient speed to keep a straight flight path, landing at the intended position on the substrate. Reis and Derby (2000) defined a parameter to assess the jettability (Z) of a given material. Z, derived from equation (1), is based on the Reynolds (Re), Weber (We) and Ohnesorge (Oh) numbers which take into account the viscous, surface tension and inertial forces on the material under jetting conditions, respectively.

$$\boldsymbol{Z} = \frac{1}{\boldsymbol{Oh}} = \frac{\sqrt{\boldsymbol{We}}}{\boldsymbol{Re}} = \frac{\sqrt{\gamma\rho L}}{\eta} \tag{1}$$

In this equation, η, γ, ρ and L represent viscosity, surface tension, density and a nominal dimension (e.g. nozzle/drop diameter), respectively. A Z-value in the 1–10 range is indicative of stable droplet production, though some researchers suggest this range may be extended. There are also other factors which affect jetting

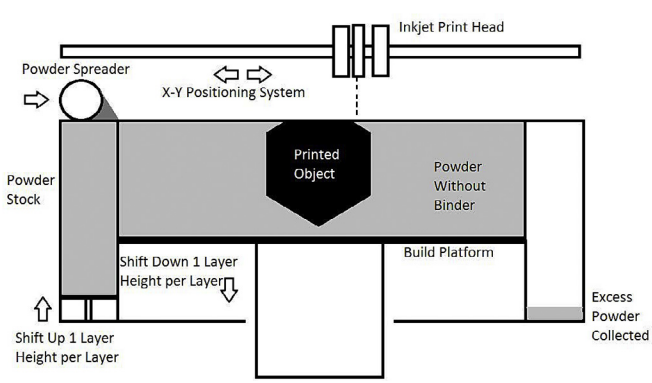

Fig. 1. Representation of the Binder Jetting Process, adapted from Gibson et al., 2010.

success, such as the molecular weight and concentration of particles or polymers contained in the ink (McIlroy et al., 2013; Soleimani-Gorgani, 2015). The application of binder jetting to food has typically utilised sugar and starch powder mixtures with water or alcohol based binders to produce macro scale, decorative 3D structures (3D Chef, 3D Systems and Walters et al., 2011). Although a useful scoping exercise in applying binder jetting to food materials, a diet in which consumption of sugary foods is high has been linked to numerous health risks such as obesity and type 2 diabetes and its reduction or substitution in the diet is being lobbied for by activist groups and governments globally (Edwards et al., 2016).

Cellulose is a major structural component within plant cell walls. It is comprised of β-(1–4) linked D-Glucose units arranged in a hierarchical series of chains to render a rigid, semi-crystalline, fibrous structure. Cellulose is naturally present in the human diet and consumed daily as part of the cell wall of any plant products however, humans do not possess the necessary enzymes to digest it so cellulose passes through the GI tract chemically unchanged, thus it is a 0kCal dietary fibre. Microcrystalline cellulose (MCC) is used as a bulk filling agent in food formulations and crystalline cellulose may be derivitized to create water soluble viscosity modifying ingredients such as carboxymethylcellulose (CMC) or methylcellulose (MC), these applications are not able to utilise cellulose as a structural or 'load-bearing' component as found in its primary role in the plant cell wall (Wuestenberg, 2014). Crystalline cellulose is used in the textiles industry; it is dissolved in ionic liquids and subsequently regenerated and recrystallized when exposed to an anti-solvent (such as water) to produce fibres which may then be woven together to create garments able to bear stresses (Rosenau et al., 2001). However, such cellulose solvents would not be suitable for food applications, but amorphisation and restructuring of cellulose into different architectures could be of interest to the food industry particularly as cellulose is a low cost, readily available ingredient. It is well documented that mechanical breakdown of crystalline cellulose via ball milling can render an amorphous cellulose powder which, under the correct conditions, may be recrystallized (Abbaszadeh et al., 2014b; Avolio et al., 2012; Hermans and Weidinger, 1946; Paes et al., 2010). Utilising this process could be a way in which cellulose is restructured in a food grade manner, and provides potential for use as a particle in ink-jet printing.

There is also interest in the interactive effects that structurally similar biopolymers (those with β-(1–4) backbone linkages) have with cellulose, particularly on controlling the formation of crystal allomorphs (Chanliaud et al., 2002; Gidley et al., 2002); xanthan gum is one such polysaccharide of interest and is also frequently used in food applications. Xanthan gum is a high molecular weight polysaccharide produced by the bacterium *Xanthomonas campestris* which exhibits very high solution viscosity at low concentrations, its solutions are also shear-thinning (Wuestenberg, 2014). Though in traditional printing applications an element of shear-thinning can aid the jetting process, non-Newtonian, high viscosity fluids due to the inclusion of a high molecular weight polymer are very difficult to ink jet print yet most food biopolymers fall into this category. Polymer chains unravel and stretch out under flow conditions, above a critical concentration or chain length this can result in the failure of an ink droplet to detach from the nozzle (McIlroy et al., 2013).

In this paper we demonstrate that an amorphous cellulose powder and a xanthan-based binder may be utilised in a 2D jetting process to create designed particles and structures for food use through controlled application of the binding agent and thermal energy. In a further 3D application, the moisture provided by the ink in combination with heat recrystallizes the amorphous powder,

Please cite this article in press as: Holland, S., et al., Design and characterisation of food grade powders and inks for microstructure control using 3D printing, Journal of Food Engineering (2017), http://dx.doi.org/10.1016/j.jfoodeng.2017.06.008

creating a crystalline network which acts as the main binding mechanism in the horizontal and vertical planes. The addition of small amounts of xanthan gum is favourable for ink jetting properties but the polymer can also act synergistically with cellulose to reinforce the binding mechanism. The resulting particle networks would have designed functionality, specifically for controlled stability or release of certain components, and 3D structures created could mimic those found in food products, such as gluten networks, but be produced from a naturally abundant, non-allergenic feedstock.

2. Experimental

2.1. Materials

The Cellulose Powder (CP) used throughout was Solka Floc 300FCC from the International Fibre Corporation, USA. It is a highly functional cellulose composed of β 1–4 glucan units sourced from a mixture of hard and softwood trees.

Xanthan Gum was provided by Danisco/DuPont Company, France. The sample had standard acetate (6.19%) and standard pyruvate (3.85%) levels (values taken from Abbaszadeh et al., 2014a).

Absolute ethanol and Tween 20 were obtained from Sigma Aldrich, UK. Grade A Ultrapure water was used in the preparation of printing inks. Red food dye introduced to inks to visualise droplets was an own-brand product from a local Sainsbury's supermarket.

2.2. Ball-mill treatment of cellulose

Milling was undertaken in a Planetary Micro Mill Pulverisette 7 (Fritsch GmbH, Germany). 1 g of a given dry sample plus six 10 mmø zirconium oxide grinding balls were used per 12 mL volume zirconium oxide pot per run. Each run consisted of 6 cycles of 5 min milling time at 800 rpm followed by 10 min pause to allow heat to dissipate to give a total milling time of 30 min. This milling regime was selected after preliminary work suggested that the powder obtained was amorphous but also had the most desirable recrystallization characteristics compared with other regimes.

2.3. Characterisation of ball milled cellulose samples

2.3.1. Scanning electron microscopy

Scanning Electron Microscopy (SEM) images were obtained using a TM3000 Table Top SEM (Hitachi High Technologies, USA). Prior to imaging, dried and powdered samples were mounted on 12.5 mmø stubs with carbon adhesive tape. These prepared samples were then platinum coated in an Emitech SC6740 Sputter Coater (Polaron Ltd, UK) to prevent charging and migration of particles during SEM.

2.3.2. Particle sizing

Particle sizing was conducted on a Mastersizer 3000 (Malvern, UK) at 1 bar air pressure with 90% feed rate and fine powder mode employed. Particles were assumed non-spherical based on visual observation through microscopy. Refractive index and absorption index were assigned values of 1.530 and 0.100 respectively based on pre-set entries for wood powder. The reported D[3,2] value was obtained from calculations within the software on measurement.

2.3.3. Wide angle X-Ray diffraction (WAXD)

Measurements were carried out on a Bruker D5005 Diffractometer (Bruker AXS, UK) using Copper K alpha (CuKα) radiation of wavelength 1.5418 Å. Samples were packed into metal holders and surfaces were smoothed with a glass microscope slide. The standard run sequence involved measuring 2θ within the angular range 3–38° at 0.05° increment step.

2.3.4. Capillary viscometry

Determination of the Degree of Polymerisation (DP) of cellulose (and thus the molecular mass) was determined through capillary viscometry. 10 mg samples of native and ball milled cellulose were dispersed in a vessel with a few lengths of copper wire and 5 mL distilled H_2O. 5 mL of 1 M Cupriethylenediamine (Cuen) was added to dissolve the cellulose suspension to give a final Cuen molarity of 0.5 M and cellulose concentration in solution of 0.1%. Full dissolution was allowed through continuous, gentle agitation on a roller bed for 2 h. 2 mL of the sample solution was loaded into a glass Ostwald U-tube capillary (App. Nr. 1069430) in a temperature-regulated water bath set to 25 °C. Flow time between two defined points was measured for a reference solvent (with no solute) and the sample solutions. This relative flow time data can then be linked to the equations mentioned in section 4.2 to determine the degree of polymerisation.

2.4. Recrystallization of ball milled cellulose

2.4.1. Dynamic vapour sorption

Water sorption isotherms were measured using a Dynamic Vapour Sorption (DVS) Analyser (Surface Measurement Systems Ltd, London, UK) with a Cahn D200 microbalance to detect sample weight changes. The standard experimental run sequence at 24 °C involved pre-drying of the initial 10 mg sample to reach equilibration at 0% Relative Humidity (RH) followed by rehydration data collection at 10% step increments from 60 to 90%RH and then at 95% RH. Equilibration was assumed when change in mass per unit time was less than 0.0005 mg min-1 or elapsed equilibration time exceeding 300 min.

2.4.2. Equilibration over saturated salt solutions

Ball milled samples were equilibrated under vacuum in a desiccator over P_2O_5 for 1 week to achieve a RH atmosphere of 2% to ensure low moisture samples. Portions of these low moisture samples were then equilibrated over NaCl (RH 75%) and $MgCl_2$ (RH 33%) at 20 °C (Rockland, 1960), chosen as RHs of interest based on the DVS data. NaCl solubility is reported as 0.37 g/mL, 50 g NaCl was dissolved in 100 mL deionised water to ensure a truly saturated solution was produced. Similarly, $MgCl_2$ solubility is reported as 0.56 g/mL; 70 g $MgCl_2 \cdot 6H_2O$ was dissolved in 100 mL deionised H_2O to produce a saturated solution.

2.4.3. Differential scanning calorimetry

Thermal transitions were monitored using a heat flux DSC 823e (Mettler Toledo, Leicester, UK) with auto sampler and liquid nitrogen cooling attachment. Samples were loaded into stainless steel pans (Perkin Elmer), hermetically sealed and run from −40 °C to 150 °C with a scan rate of 10 °Cmin^{-1} with a subsequent cooling at 50 °Cmin^{-1} and holding time for 5 min at −40 °C then a reheat step.

2.4.4. Sample recrystallization

Equilibrated samples were packed into 10 μL aluminium crucibles (usually used for Thermal Gravimetric Analysis) and hermetically sealed (in duplicate). Based on thermal analysis, a water bath was prepared corresponding to the temperature after the observed crystallization for a particular sample (typically close to 80 °C). These pans were then submerged in the water bath for 2 min to allow full heat transfer through the sample. Powders were removed from the pans and analysed using WAXD to determine the extent of recrystallization.

Please cite this article in press as: Holland, S., et al., Design and characterisation of food grade powders and inks for microstructure control using 3D printing, Journal of Food Engineering (2017), http://dx.doi.org/10.1016/j.jfoodeng.2017.06.008

2.5. Ink formulation

2.5.1. Ball mill treatment of xanthan gum

Ball milling was undertaken in the same manner as described in section 3.2, however, cycle repetitions were increased to give a total milling time of 60 min and one sample was run at 400 rpm, the other at 800 rpm.

2.5.2. Ink formulations

Native XG and ball milled XG (as prepared in section 3.5.1) were dissolved in ultrapure water to create stock solutions of 0.5%wt concentration. From these, three ink formulations were prepared:

2.5.3. Rheological measurement

Ink flow curves were developed using a MCR301 rheometer (Anton Parr, Austria) with double gap geometry. Shear rate was varied logarithmically from 0.1 to 1000s^{-1} with 7 measuring points per decade, measurement time intervals were varied initially set to 10s and ending at 1s. The system was kept at 30 °C throughout with 2 min equilibration time allowed prior to shearing. Samples were measured in triplicate and 100 cSt silicone oil (Dow Corning, USA) used as a standard prior to measurements on different days.

2.5.4. Surface tension measurement

Drop shape analysis and surface tension were measured via the pendant drop method using a Drop Shape Analyser DSA100S (Krüss GmbH, Germany). Once the droplet profile was extracted the software calculated a surface tension value using the Young-Laplace equation. Pure water was used as a standard prior to each set of measurements.

2.5.5. Solution density

Density was determined using a density and sound velocity meter, DSA 5000 M (Anton Parr, Austria). Samples were introduced to the oscillating U-Tube with a syringe. The density was measured in triplicate, a new aliquot was then introduced and measured in triplicate again. Pure water was used to calibrate the machine prior to each use.

2.6. Printing ink onto powder

All printing was done using a Dimatix DMP-2831 ink jet printer (FujiFilm, USA). The print cartridge temperature remained at 30 °C and platen temperature varied depending on the substrate. Initial printability assessments of the ink formulations were carried out using the drop watcher function and then onto standard A4 paper to serve as a porous material substitute for the powder.

A bespoke recessed plate was designed and machined out of aluminium with two rows of four 10 × 10 mm square wells. One row of wells had a constant depth of 100 μm deep, the row beneath it had wells of sequentially increasing depth from 100 to 400 μm. To enable ease of spreading powder was passed through a 100 μm sieve prior to use so that no particle had larger dimensions than the set layer thickness. Powder was loaded into the wells with a glass microscope slide, similar to WAXD, with care to keep powder packing consistent. Patterns were then designed using the Dimatix software and printed onto the powder samples.

2.6.1. Optical characterisation

An Eclipse LV100ND (Nikon UK Ltd.) was used to observe powder-binder interactions after printing.

3. Theory/calculations

3.1. Cellulose crystallinity

Crystallinity determination followed the curve fitting approach taken by Paes et al. (2010) and Winkworth-Smith (2014) using Microsoft Excel software with solver add-in. Diffraction peaks corresponded to crystallographic planes 110, 1$\bar{1}$ 0, 021 and 200 typical of cellulose I and 110, 1$\bar{1}$ 0 and 020 typical of cellulose II (2θ~12°, 14.5°, 16.6°, 20°, 20.4°, 21.5° and 22.5°) and were simulated as pure Gaussian functions along the x axis. One broad Gaussian feature was used to represent the amorphous background of the material (2θ ~ 18.4°) (Poletto et al., 2014; Sèbe et al., 2012; Winkworth-Smith, 2014).

3.2. Cellulose degree of polymerisation

Raw data obtained through capillary viscometry (see section 3.3.4) was manipulated to obtain the sample intrinsic viscosity [η] as per equations (8)–(11) used by Oberlerchner et al. (2015).

$$[\eta] = \boldsymbol{KD_P} \tag{2}$$

The Mark-Houwink-Sakurada (MHS) equation was then used to determine the viscosity average Degree of Polymerisation (DP) of the cellulose samples tested. K and α are empirical constants obtained from literature relating to the dissolution of a particular solute in a defined solvent at a given temperature. These values vary substantially in the literature In addition to the 5 sets of literature values tabulated by Winkworth-Smith (2014) values recently reported by Kes and Christensen (2013) as K = 2.45 and α = 0.70 were considered before the latter were chosen as MHS constants to be used throughout this work as they are shown to be valid for cellulose samples with any chain length distribution dissolved in Cuen. If desired, the viscosity average molecular weight of a sample can be determined by multiplying the DP value by the molecular weight of an anhydroglucose molecule (162 g mol^{-1}).

3.3. Statistical analysis

Statistical analysis of data was performed on XLSTAT v2016.04 (Addinsoft, Paris). Data comparing native and ball milled cellulose from Table 1 was tested for significance using a student t-test. Table 2 containing data on ink printability parameters was tested for significance and interactions with ANOVA and a post-hoc Tukey HSD test.

4. Results

4.1. Powder characterisation

Ball milling was shown to alter and significantly decrease ($p < 0.05$ based on *t*-test) three measured properties of native cellulose; particle size/morphology, degree of polymerisation (DP)

Formulation	Water (wt%)	Ethanol (wt%)	Tween 20 (wt%)	Xanthan (wt%)
0.25%Native	79.25	20	0.5	0.25
0.25%BM400 rpm,60min	79.25	20	0.5	0.25
0.25%BM800 rpm,60min	79.25	20	0.5	0.25

Please cite this article in press as: Holland, S., et al., Design and characterisation of food grade powders and inks for microstructure control using 3D printing, Journal of Food Engineering (2017), http://dx.doi.org/10.1016/j.jfoodeng.2017.06.008

Table 1
Characterisation of differences between native cellulose and cellulose ball milled at 800 rpm for 30 min.

	Particle size d[3,2] (μm)	Degree of polymerisation (DP)	Type I (%)	Crystallinity type II (%)	Overall (%)
Native SF300	16 ± 0.2[a]	1339 ± 51[a]	25	0	25[a]
Ball Milled 800 rpm 30min	13 ± 0.1[b]	411 ± 59[b]	2	4	6[b]

a, b (denotes significantly different values $p < 0.05$ according to student t-test).

Table 2
Jettability Parameter (Z) for inks with Xanthan Gum and key parameters necessary to calculate this value.

Ink formulation	Viscosity at $1000s^{-1}$ and 30 °C (mPa.s)	Density (gcm^{-3})	Surface tension (mNm^{-1})	Z
0.25% Native XG	1.6 ± 0.02[a]	$0.974 \pm 2 \times 10^{-6}$ [a]	37 ± 1.0[a]	17[a]
0.25%BM400 rpm,60min	1.8 ± 0.04[b]	$0.973 \pm 5 \times 10^{-7}$ [b]	35 ± 1.0[b]	15[b]
0.25%BM800 rpm,60min	1.7 ± 0.00[b]	$0.972 \pm 7 \times 10^{-7}$ [c]	35 ± 1.0[b]	15[b]

a, b (denotes significantly different values $p < 0.05$ according to Tukey pairwise comparison test).

and crystallinity, the results of which are summarised in Table 1.

The D[3,2] value obtained for particle size refers to the ratio of volume to surface area and reflects the loss of the high aspect ratio, fibrillar morphology as seen in Fig. 2. In addition, the selected ball milling regime was shown to decrease the viscosity average DP of cellulose molecules to $^1/_3$ of the starting value, which correlates with a plateau value observed by Winkworth-Smith (2014) when ball milling various cellulose samples for different lengths of time (note that alternative values for empirical constants were used between studies). The reduction in overall crystallinity (as an accumulation of type I and II allomorphs) achieved was to <5%. The ball milled sample is a broad, featureless, amorphous curve; it lacks the characteristic crystalline peaks of native cellulose at those values of 2θ outlined in section 4.1. The amorphous nature of this sample compared with the native cellulose was confirmed both by solid state NMR spectra and the loss of birefringence under polarised light of the ball milled sample (data not presented).

Dynamic Vapour Sorption (DVS) showed that, at 25 °C temperature, the ball milled cellulose recrystallized when held in an environment above 90% relative humidity (RH). The sorption isotherms are not shown in this work, but enabled the selection of NaCl and $MgCl_2$ as ambient equilibration salts to control sample moisture content but not recrystallize without sufficient heat input in the observed time period. Differential Scanning Calorimetry (DSC) of ball milled samples over the different equilibration salts provided information on the recrystallization temperature onset, in Fig. 3, the peak of interest is enclosed between solid lines. For the sample equilibrated over NaCl (75%RH) this recrystallization peak had merged with the generic polymer relaxation peak,

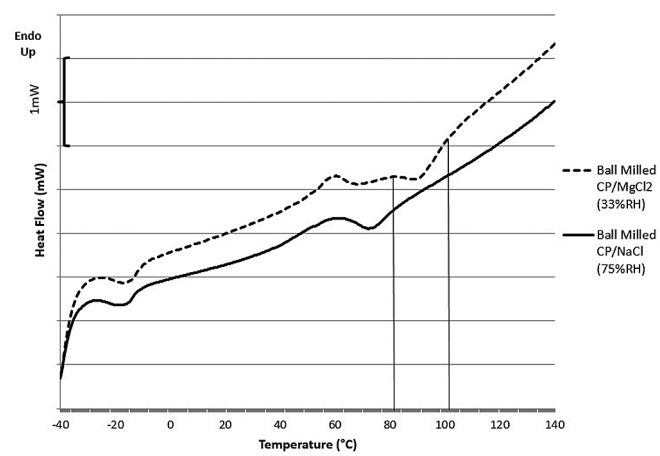

Fig. 3. DSC traces of ball milled cellulose stored over two saturated salt solutions.

by equilibrating at a lower RH (thus giving the sample a lower moisture content) it was possible to separate these peaks and deduce an approximate onset temperature of 80 °C when equilibrated over $MgCl_2$ (33%RH). This data can be extrapolated when looking at a 3D process to identify heating parameters. The number of drops (and thus their volume) deposited over a given area and depth of powder may be calculated. Thus the ratio of powder to binder in the process can be deduced and a temperature known to recrystallize amorphous cellulose at that moisture content can be selected.

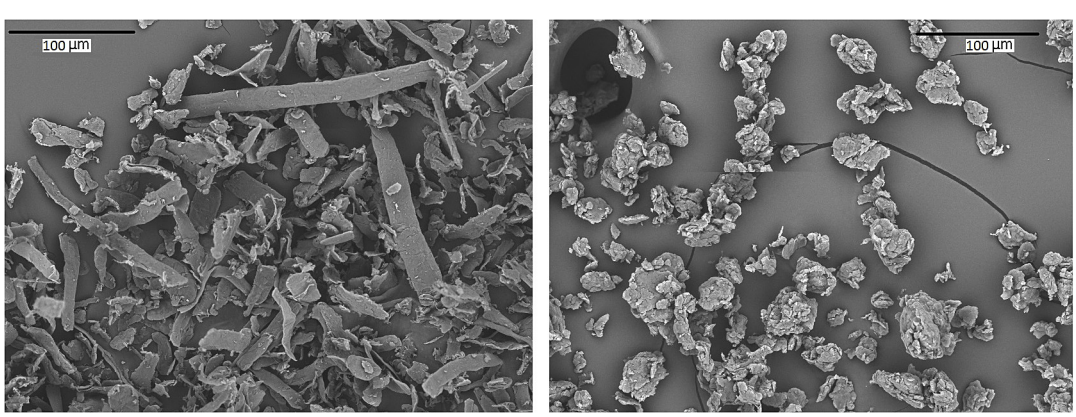

Fig. 2. Scanning Electron Micrographs of native cellulose (left) and the ball milled sample (right).

Please cite this article in press as: Holland, S., et al., Design and characterisation of food grade powders and inks for microstructure control using 3D printing, Journal of Food Engineering (2017), http://dx.doi.org/10.1016/j.jfoodeng.2017.06.008

4.2. Ink characterisation

Inks were formulated by varying the levels of solvent (pure water and ethanol), surfactant (Tween 20) and xanthan gum solution. By changing ink composition as well as using varying ball mill treatments on the xanthan gum as an attempt to reduce its molecular weight the viscosity could be altered, as per Fig. 4. Fig. 4A illustrates that at low shear ($1s^{-1}$) a 0.5% solution of native XG in water exhibits a higher viscosity (2.45 Pa s). Ball milling at 400 rpm for 60 min decreased the viscosity slightly to 1.72 Pa s but a harsher milling regime at 800 rpm for 60 min substantially reduced viscosity to 0.3 Pa s retaining the same concentration in solution. It is widely regarded that viscosity is related to XG, or any polymer, molecular weight (Erten et al., 2014; Mezger, 2015). Under high shear conditions ($1000s^{-1}$), however, apparent solution viscosities are similar (0.01 ± 0.002 Pa s). In Fig. 4B the same trend is observed for ink formulations made with ball milled XG at a concentration of 0.25%.

It was found that the addition of 0.5% Tween 20 gave a surface tension value suitable for printing (which for the Dimatix is 28–42 mN m^{-1} (Fujifilm, 2010), as hypothesised from work by Kothekar et al. (2007). However, measured surface tension values were significantly different ($p < 0.05$) between both inks containing milled XG and the ink with native XG. It is possible that low molecular weight fragments produced during the milling regimes are interacting at the surface differently to the high molecular weight native XG. All measured properties determining the supposed 'jettability' parameter of the inks are displayed in Table 2.

As stated in the introduction, a Z-value between 1 and 10 indicates the ability to form stable, singlet droplets. Table 2 shows the calculated Z-value of the inks with xanthan gum, based on the measured viscosity, surface tension and density. Overall the inks containing ball milled XG were significantly different to the ink with native XG as determined by Tukey pairwise comparison testing. Though both ball milled samples were grouped the same and interaction was identified between milling rpm and time affecting all measurements (μ, ρ and γ). Using an online tool developed by Abbott (2016), based on work by Derby (2010), whereby the Z parameter is plotted against the Reynold's number (Re) it is possible to predict the jetting profile of inks. These inks fall just outside the optimal jetting zone and would be likely to produce satellite droplets, as demonstrated by the marker falling just outside the optimal grey area in Fig. 5. However, using waveforms developed to suit low viscosity inks and optimising jetting voltage and frequency through visual observation using the Drop Watcher function, stable droplets were able to be formed by a sufficient number of adjacent nozzles to allow material jetting, shown on the right hand side of this figure. Due to the similarity of the Z parameter for each ink, differences in the quality of droplets produced and printing success can be attributed to the chain length of xanthan gum contained in the ink. Polymer chain length and conformation has been identified by McIlroy (2014) as an additional factor to viscosity to be aware of when designing jetting inks. In Fig. 4a, xanthan gum that has been ball milled exhibits lower viscosity at low shear in a 0.5% solution compared with native xanthan which can be linked to a decrease in molecular weight as a result in the milling process. Therefore, it is hypothesised that if the molecular weight of each milled XG solution were to be measured that this parameter would differentiate the inks in Table 2 into three significantly different groupings. It is favourable to have smaller polymers in solution to prevent stretching under high shear during printing, resulting in either failure of the droplet to detach from the nozzle or molecular scission.

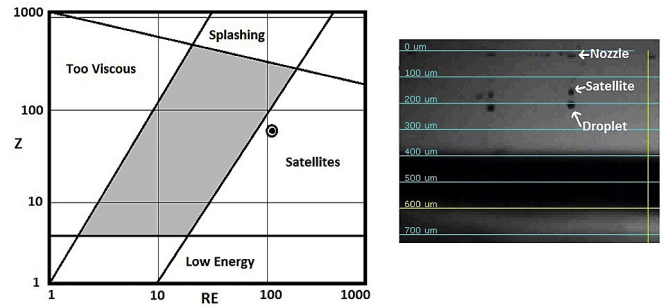

Fig. 5. Left: Interactive Jettability Model (redrawn from the online interactive tool developed by Abbott (2016)) indicating potential for satellite droplet formation given the calculated Z value for an ink with xanthan gum Right: Evidence of satellite droplets when using the Dimatix Drop Watcher on an ink formulation. The increments on the left hand side indicate distance from the nozzle and can be used to calculate droplet speed whilst using the real time movie function.

4.3. Cellulose recrystallization through printing

To confirm the existence of this controllable recrystallization mediated by temperature and moisture the hermetically sealed, heated samples were analysed by WAXD, as described in the methods section. Fig. 6 shows diffractograms and total crystallinity values of native cellulose, ball milled cellulose stored over P_2O_5 desiccant, a ball milled sample stored over NaCl then recrystallized by being hermetically sealed and subjected to heat treatment and, finally, a low moisture sample with controlled addition of an ink formulation heated at 65 °C. The original crystallinity of the cellulose is almost totally recovered when the environmental conditions of moisture and heat are controlled.

Food dye was added to inks to allow easier visualisation of the ink on powder. At concentrations used the dye addition affected ink viscosity at $0.1s^{-1}$ but not at $1000s^{-1}$, the shear rate taken into account in this study as relevant to the ink jetting process. Ball

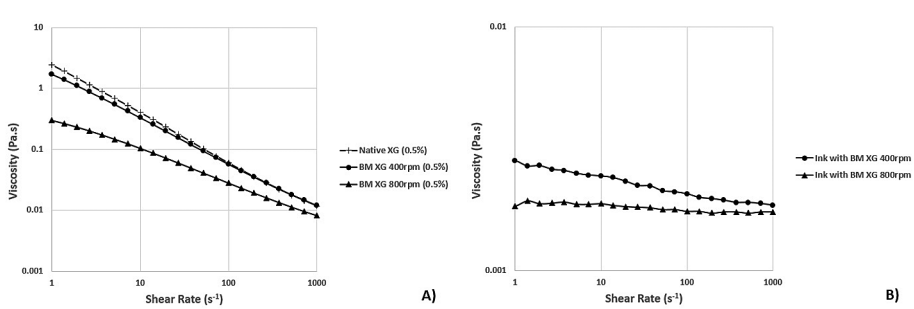

Fig. 4. Flow curves of A) 0.5% Solutions of Native Xanthan Gum and two different ball milled samples and B) These samples present in ink formulations with equal water, ethanol and surfactant.

Please cite this article in press as: Holland, S., et al., Design and characterisation of food grade powders and inks for microstructure control using 3D printing, Journal of Food Engineering (2017), http://dx.doi.org/10.1016/j.jfoodeng.2017.06.008

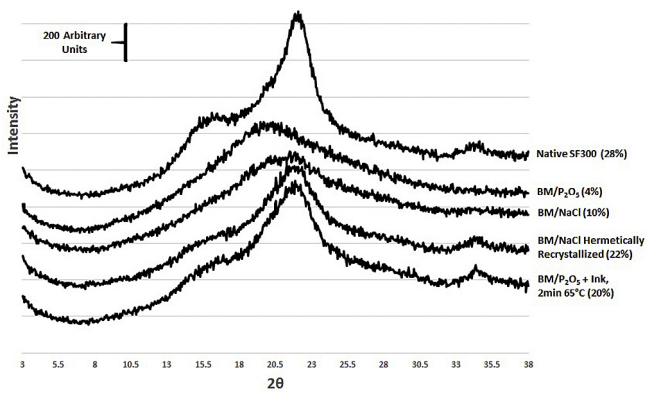

Fig. 6. WAXD and crystallinity data for native cellulose; ball mill treated cellulose stored over P2O5 and NaCl; Ball milled cellulose recrystallized when hermetically sealed and using the recessed plate (calculated crystallinity shown in parantheses).

milled cellulose powder was loaded into the 100 μm recessed plate wells and varying layers of ink were deposited in 5 × 5mm square patterns. It was found that only depositing one layer of droplets was not sufficient to produce a cohesive powder layer able to be lifted cleanly. Three, five and ten ink layers applied to the powder produced structures that were able to withstand transfer onto glass microscope slides to varying degrees.

Fig. 7 shows macroscopic and microscopic images of an ink-powder system. It is evident that the pattern edges formed are of a good resolution and that the droplet spacing selected forms clear lines rather than discrete droplets on the powder. The pattern could be lifted away from the unbound powder and, though it showed a brittle nature, it remained intact. If these 2D films were layered, a 3D cube could be formed. Due to the freedom of design possible with such a process more complex patterns could be created for 3D application.

5. Conclusions and future work

Optimised ball mill treatment of native, semi-crystalline cellulose was able to render an amorphous powder product, as determined by WAXD and solid state NMR, which could be spread in layers. Thermal analysis showed that the powder could be recrystallized through mediation of moisture and temperature applied.

Through manipulation of rheological properties, surface tension and material density, food grade inks were developed that possessed the necessary properties to be successfully ink jet printed in a Fujifilm Dimatix printer.

By controlling the temperature of both the ink cartridge and substrate, then varying the number of ink layers deposited onto the powder, cohesive 2D structures were produced.

The next stage of this work is to apply the materials to a 3D process by alternating powder and ink layers *in situ*, as has been demonstrated in this 2D scenario. The system can be subjected to post-printing heat treatment to selectively recrystallize the powder that has had ink printed on it, thus enabling a cohesive 3D cellulose structure to be obtained. To enhance powder cohesion other β-(1–4) linked polysaccharides can be incorporated into the powder phase, which will also allow for different end material properties. Once basic printing and heating parameters are optimised more complex formulations and structure designs may be used in the process to create functional ingredients for food products, for example; novel textures, lattices and composite particles.

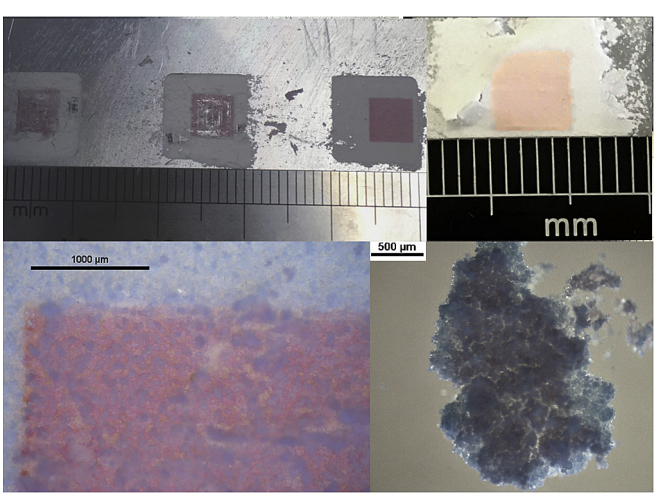

Fig. 7. Clockwise from top left: Ball Milled Cellulose powder in recessed plate with varying printed ink layers; Ball Milled cellulose with 10 ink layers on glass microscope slide; Optical microscopy of ball milled cellulose with printed ink particle; Optical microscopy of square printed pattern on cellulose powder.

Acknowledgements

The authors would like to thank the support of Dr. Bettina Wolf (Division of Food Science) and Dr. Phill Dickens (3DP and AM Research Group) for stimulating discussions regarding this work.

References

3D Chef (Julian Sing). Available Online: [https://3dchefblog.wordpress.com/] Accessed on: 16 April 2016.

3D Systems. Culinary Collaborations. Available Online: [http://www.3dsystems.com/culinary] Accessed on: 25 August 2015.

Abbaszadeh, A., Lad, M., Janin, M., Morris, G.A., MacNaughtan, W., Sworn, G., Foster, T.J., 2014a. A novel approach to the determination of the pyruvate and acetate distribution in xanthan. Food Hydrocoll. 44, 162–171. http://dx.doi.org/10.1016/j.foodhyd.2014.08.014.

Abbaszadeh, A., Macnaughtan, W., Foster, T.J., 2014b. The effect of ball milling and rehydration on powdered mixtures of hydrocolloids. Carbohydr. Polym. 102, 978–985. http://dx.doi.org/10.1016/j.carbpol.2013.10.020.

Abbott, S., 2016. Ohnesorge for Ink Jet. Available Online. http://www.stevenabbott.co.uk/practical-coatings/ohnesorge.php. Accessed 8 August 2016.

ASTM International, 2015. ISO/ASTM52900–15. Standard Terminology for Additive Manufacturing – General Principles – Terminology. ASTM, West Conshohocken, PA.

Avolio, R., Bonadies, I., Capitani, D., Errico, M.E., Gentile, G., Avella, M., 2012. A multitechnique approach to assess the effect of ball milling on cellulose. Carbohydr. Polym. 87 (1), 265–273. Available at: http://dx.doi.org/10.1016/j.carbpol.2011.07.047.

Chanliaud, E., Burrows, K.M., Jeronimidis, G., Gidley, M.J., 2002. Mechanical Properties of Plant Cell Wall Analogues. Planta. 215, 989–996.

Derby, B., 2010. Inkjet printing of functional and structural materials: fluid property requirements, feature stability, and resolution. Annu. Rev. Mater. Res. 40, 395–414.

D'Angelo, G., Hansen, H.N., Hart, A.J., 2016. Molecular gastronomy meets 3D printing: layered construction via reverse spherification. 3D print. Addit. Manuf. 3, 152–159.

Edwards, C., Rossi, M., Corpe, C., Butterworth, P., Ellis, P., 2016. The Role of Sugars and Sweeteners in Food, Diet and Health: Alternatives for the Future, 56. Trends in Food Science and Technology, pp. 158–166. Available online: http://www.sciencedirect.com/science/article/pii/S0924224415301539.

Erten, T., Adams, G.G., Foster, T.J., Harding, S.E., 2014. Comparative heterogeneity, molecular weights and viscosities of xanthans of different pyruvate and acetate content. Food Hydrocoll. http://dx.doi.org/10.1016/j.foodhyd.2014.04.012.

Fujifilm, 2010. FUJIFILM Dimatix Materials Printer User Manual.

Gibson, I., Rosen, D., Stucker, B., 2010. Additive Manufacturing Technologies. 3D Printing, Rapid Prototyping and Direct Digital Manufacturing, second ed. Springer-Verlag, New York.

Gidley, M.J., Chanliaud, E., Whitney, S., 2002. Influence of Polysaccharide Composition on the structure of Cellulose-Based Composites in Plant Biopolymer Science: Food and Non-Food Applications eds. In: Renard, D., Della Valle, G., Popineau, Y. (Eds.). Royal Society of Chemistry, GB, pp. 39–47.

Godoi, F.C., Prakash, S., Bhandari, B.R., 2016. 3d printing technologies applied for food design: status and prospects. J. Food Eng. 179, 44–54. http://dx.doi.org/

ARTICLE IN PRESS

10.1016/j.jfoodeng.2016.01.025.
Hamilton, C.A., Alici, G., In Het Panhuis, M., 2017. 3D Printing Vegemite and Marmite: Redefining " Breadboards ", pp. 6–11. http://dx.doi.org/10.1016/j.jfoodeng.2017.01.008.
He, Y., Qiu, J., Fu, J., Zhang, J., Ren, Y., Liu, A., 2015. Printing 3D microfluidic chips with a 3D sugar printer. Microfluid. Nanofluidics 19, 447–456. http://dx.doi.org/10.1007/s10404-015-1571-7.
Hermans, P.H., Weidinger, A., 1946. On the recrystallization of amorphous cellulose. Laboratory Cellul. Res. AKU Affil. Co. 68, 2547–2552.
Kes, M., Christensen, B.E., 2013. A re-investigation of the Mark-Houwink-Sakurada parameters for cellulose in Cuen: a study based on size-exclusion chromatography combined with multi-angle light scattering and viscometry. J. Chromatogr. A 1281, 32–37.
Kothekar, S., Ware, A., Waghmare, J., Momin, S., 2007. Comparative analysis of the properties of Tween-20, Tween-60, Tween-80, Arlacel-60, and Arlacel-80. J. Dispersion Sci. Technol. 28 (3), 477–484.
Le Tohic, C., O'Sullivan, J.J., Drapala, K.P., Chartrin, V., Chan, T., Morrison, A.P., Kerry, J.P., Kelly, A.L., 2017. Effect of 3D printing on the structure and textural properties of processed cheese. J. Food Eng. http://dx.doi.org/10.1016/j.jfoodeng.2017.02.003.
Lipton, J., Cutler, M., Nigl, F., Cohen, D., Lipson, H., 2015. Additive manufacturing for the food industry - a review. Trends Food Sci. Technol. 43 (1), 114–123. Available at: http://www.sciencedirect.com/science/article/pii/S092422441500045X.
McIlroy, C., Harlen, O.G., Morrison, N.F., 2013. Modelling the jetting of dilute polymer solution in drop-on-demand inkjet printing. J. Newt. Fluid Mech. 201, 17–28.
McIlroy, C., 2014. Complex Inkjets: Particles, Polymers and Non-Linear Driving. PhD. University of Leeds. Available at: http://etheses.whiterose.ac.uk/7732/1/ClaireThesis.pdf.
Mezger, Thomas G., 2015. Flow behaviour, flow curve and viscosity curve. In: Applied Rheology. Anton Paar GmbH, Austria, pp. 31–46.
Oberlerchner, J.T., Rosenau, T., Potthast, A., 2015. Overview of methods for the direct molar mass determination of cellulose. Molecules 20, 10313–10341. Available at: http://www.mdpi.com/1420-3049/20/6/10313/.
Paes, S., Sun, S., MacNaughtan, W., Ibbett, R., Ganster, J., Foster, T.J., Mitchell, J.R., 2010. The glass transition and crystallization of ball milled cellulose. Cellulose 17, 693–709. Available at: http://link.springer.com/10.1007/s10570-010-9425-7.
Poletto, M., Ornaghi Jr., H.L., Zattera, A.J., 2014. Native cellulose: structure, characterization and thermal properties. Materials 7, 6105–6119.
Reis, N., Derby, B., 2000. Ink jet deposition of ceramic suspensions: modelling and experiments of droplet. In: MRS Proceedings, vol. 624, pp. 65–70.
Rockland, L.B., 1960. Saturated salt solutions for static control of relative humidity between 5 and 40 C. Anal. Chem. 32, 1375–1376. http://dx.doi.org/10.1021/ac60166a055.
Rosenau, T., Potthast, A., Sixta, H., Kosma, P., 2001. The chemistry of side reactions and byproduct formation in the system NMMO/cellulose (Lyocell process). Prog. Polym. Sci. 26, 1763–1837. https://doi.org/10.1016/S0079-6700(01)00023-5.
Sèbe, G., Ham-Pichavant, F., Ibarboure, E., Koffi, A.L.C., Tingaut, Ps, 2012. Supramolecular structure characterization of cellulose II nanowhiskers produced by acid hydrolysis of cellulose I substrates. Biomacromolecules 13, 570–578.
Shirazi, S., Gharehkhani, S., Mehrali, M., Yarmand, H., Metselaar, H., Adib Kadri, N., Osman, N., 2015. A review on powder-based additive manufacturing for tissue engineering: selective laser sintering and inkjet 3D printing. Sci. Technol. Adv. Mater. 16 (3).
Soleimani-Gorgani, A. (2015) Ink Jet Printing Chapter: 14 in book: Printing on Polymers: Fundamentals and Applications, Publisher: Elsevier, Editors: Izdebska, J. and Thomas, S. pp.231–245.
Sun, J., Zhou, W., Huang, D., Fuh, J.Y.H., Hong, G.S., 2015. An overview of 3D printing technologies for food fabrication. Food Bioprocess Technol. 8, 1605–1615. Available at: http://link.springer.com/10.1007/s11947-015-1528-6.
Sun, J., Zhou, W., Yan, L., Huang, D., Lin, L., 2017. Extrusion-based food printing for digitalized food design and nutrition control. J. Food Eng. 1–11. http://dx.doi.org/10.1016/j.jfoodeng.2017.02.028.
Vorndran, E., Moseke, C., Gbureck, U., 2015. 3D printing of ceramic implants. MRS Bull. 40, 127–136.
Walters, P., Huson, D., Southerland, D., 2011. Edible 3D printing. In: Society for Imaging Science and Technology, Ed. (2011) NIP27: International Conference on Digital Printing Technologies and Digital Fabrication 2011. (27). The Society for Imaging Science and Technology, USA, pp. 819–822. ISBN 978892082964 Available from: http://eprints.uwe.ac.uk/15349.
Wegrzyn, T.F., Golding, M., Archer, R.H., 2012. Food Layered Manufacture: a new process for constructing solid foods. Trends Food Sci. Technol. 27, 66–72. Available at: http://dx.doi.org/10.1016/j.tifs.2012.04.006.
Winkworth-Smith, C.G., 2014. Cellulose Composite Structures – by Design. Unpublished PhD Thesis. The University of Nottingham.
Wuestenberg, T., 2014. Cellulose and Cellulose Derivatives in the Food Industry: Fundamentals and Applications. John Wiley and Sons Ltd, United Kingdom.

Please cite this article in press as: Holland, S., et al., Design and characterisation of food grade powders and inks for microstructure control using 3D printing, Journal of Food Engineering (2017), http://dx.doi.org/10.1016/j.jfoodeng.2017.06.008